MARCEL DEKKER, INC. • 270 MADISON AVENUE • NEW YORK, NY 10016

MECHANICS BASED DESIGN OF STRUCTURES AND MACHINES
Vol. 31, No. 2, pp. 151–179, 2003

Design of Distributed Compliant Mechanisms

Luzhong Yin and G. K. Ananthasuresh*

Department of Mechanical Engineering and Applied Mechanics, University of Pennsylvania, Philadelphia, Pennsylvania, USA

ABSTRACT

The optimization problem formulations currently used to synthesize compliant mechanism topologies aim to maximize the flexibility for obtaining the desired output motion while maximizing the overall stiffness for satisfactorily bearing the applied loads. The best solution to this problem, as posed, is a linkage consisting of rigid members connected together with revolute joints. The current elastic mechanics-based formulations do generate compliant topologies that closely imitate a rigid-body linkage by means of lumped compliance as in flexural pivots. Systematically generating such topology solutions could serve as a creative aid in the conceptual design of mechanisms, especially when the force-deflection specifications are

*Correspondence: G. K. Ananthasuresh, Department of Mechanical Engineering and Applied Mechanics, University of Pennsylvania, 297 Towne Building, 220 South 33rd Street, Philadelphia, PA 19104-6315, USA; Fax: (215) 573-6334; E-mail: gksuresh@seas.upenn.edu.

DOI: 10.1081/SME-120020289 1539-7734 (Print); 1539-7742 (Online)

nonintuitive to human designers. However, flexural pivot-based compliant designs are not useful in most applications when large displacements and/or high strength are desired. Ideally, compliant designs should distribute flexibility uniformly throughout the structure rather than limiting it to a few pivots. In this article, we discuss why current formulations often lead to lumped compliant designs, put forth a proper quantitative measure for distributed compliance, and present a novel formulation that guarantees distributed compliant topologies. The method is explained in detail and is illustrated with examples.

INTRODUCTION

Compliant mechanisms rely upon elastic deformation to perform their function of transmitting and/or transforming motion and force (Her and Midha, 1987). From an overall perspective that considers performance, manufacturability, economy of material, scalability to micro and nano sizes, adaptability to smart actuations and embedded sensors, resistance to wear, etc., compliant mechanisms are preferable over rigid-body mechanisms. In spite of their numerous attractive attributes, compliant mechanisms were not used as widely as rigid-body mechanisms in the past. One reason for this might be the lack of materials and processing techniques that enable structures that can deform considerably with adequate strength. This is changing as new materials and manufacturing techniques become available. The other reason might be the lack of systematic design techniques for compliant mechanisms. Extensive research done in the last 15 years has addressed this need. Furthermore, there are certain applications such as micro and nano systems where compliant designs are indeed essential (Ananthasuresh and Kota, 1995). Consequently, the application domain of compliant mechanisms (Howell, 2001) continues to expand with better materials and processing techniques, design methods, and specialized needs of emerging areas of engineering and science. The focus of this article is on furthering the design of compliant mechanisms.

Currently available design techniques for compliant mechanisms can be grouped broadly into the following three categories based on the methods used as well as the type of mechanisms created using them.

- Flexural pivot-based compliant mechanisms.
- Flexible beam-based compliant mechanisms.
- Fully compliant, elastic continua.

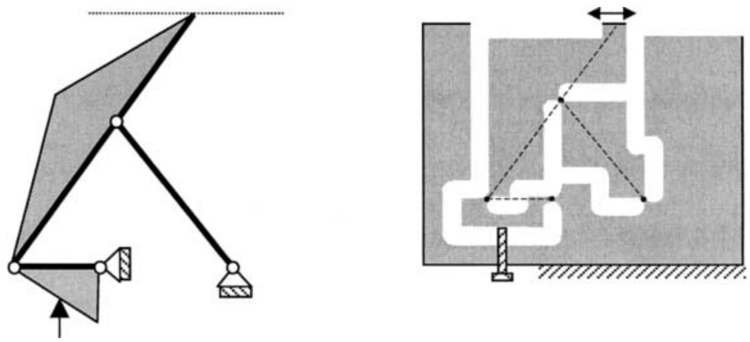

Figure 1. A flexural pivot-based compliant mechanism derived from a cognate of the Chebyshev's approximate straight-line linkage.

Flexural pivot-based designs use narrow sections connecting relatively rigid segments. Thus, compliance is lumped to a few portions of the mechanism. They are usually of monolithic construction. They can be systematically designed either by starting from an available rigid-body linkage or an intuitively conceived linkage (Forster, 2000; Smith and Chetwynd, 1994) or by synthesizing a rigid-body linkage that includes torsional springs at the joints to model the flexural pivots (Howell and Midha, 1994). An example is shown in Fig. 1, wherein a cognate of Chebychev's approximate straight-line linkage (Waldron and Kinzel, 2000) has been transformed to a monolithic compliant mechanism with flexural pivots. As can be seen in the figure, flexural pivots are easy to manufacture. The techniques for designing them have been available for a long time (Paros and Weisbord, 1965), and some improvements are still being pursued (Lobontiu et al., 2001). Compliant mechanisms of this type are often restricted to a small range of motion. Their applications are in precision instrumentation (Smith and Chetwynd, 1994; Tuttle, 1967) and many consumer products.

Flexible beam-based compliant designs extend the range of motion because the slender beam-like segments are designed to undergo large deformations (Burns and Crossley, 1968; Howell and Midha, 1996; Mettlach and Midha, 1996; Shoup and McLarnan, 1971). These are not always of monolithic construction, as they may have some rigid segments and kinematic joints. Thus, they are sometimes partially compliant. Unlike in flexural pivot-based designs, the compliance is distributed in flexible beam-based designs. Traditional kinematic analysis and synthesis techniques are applicable to them when the compliance in beams is modeled using the theory of undulating elastica (Shoup and McLarnan, 1971) or a rigid-link approximation of a cantilever beam (Burns and Crossley, 1968) or a more recently developed pseudo rigid-body model (Howell, 2001; Howell and Midha, 1996; Mettlach and Midha, 1996).

Further generalization of distributed compliant mechanisms leads to monolithic elastic continua designed to deform in the desired manner under applied loads. Techniques for designing them utilize topology optimization (Frecker et al., 1997; Nishiwaki et al., 1998; Saxena and Ananthasuresh, 2000; Sigmund, 1997). In topology optimization, a variable assigned to every point in the design region is varied smoothly between its "existence" and "nonexistence" states, thus converting the topology optimization to a material distribution problem on a fixed reference domain. Using only function-level specifications, such as the ones shown in Fig. 2a, a compliant topology is generated as shown in Fig. 2b.

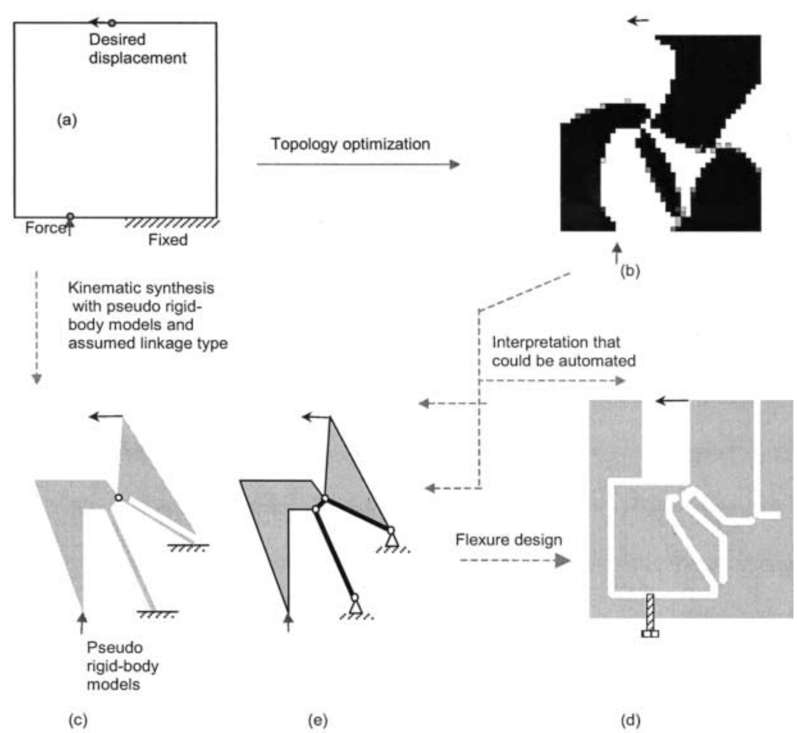

Figure 2. A summary of available design techniques for compliant mechanisms (a) specifications; (b) topology solution; (c) partly compliant mechanism; (d) compliant mechanism with flexures; (e) rigid-body linkage. Dashed green lines with arrows indicate that design techniques are now available to go in that direction.

From this topology, the other two types of compliant mechanisms can be derived if it is so desired (Figs. 2c and 2d). And, indeed, rigid-body linkages can be deduced as well (Fig. 2e) (Saxena and Ananthasuresh, 2002). Thus, on the one hand, the topology optimization serves as a creative design tool, and, on the other, the generated compliant topologies have sufficient detail to automatically generate instructions for manufacturing equipment at the macro or micro scale. The solution shown in Fig. 2b was obtained with linear elastic modeling assuming small deformations. Extensions to large deformations (Bruns and Tortorelli, 2001; Pedersen et al., 2001; Saxena and Ananthasuresh, 2001a), inclusion of stress constraints (Duysinx and Bendsøe, 1998; Saxena and Ananthasuresh, 2001b), designing with multiple materials (Yin and Ananthasuresh, 2001), and nonmechanically actuated structures (Sigmund, 2001; Silva et al., 2000; Yin and Ananthasuresh, 2002) have also been demonstrated.

Motivation

As can be seen in Fig. 2, the optimal continuum topology obtained using a method described in Saxena and Ananthasuresh (2000), turned out to be a lumped compliant mechanism, although that was not the intent. This is not an isolated case but is actually quite representative (Frecker et al., 1997; Nishiwaki et al., 1998; Saxena and Ananthasuresh, 2000; Sigmund, 1997; see especially Saxena et al., 2000; TOPOPT). This is true with both continuum design parameterization (e.g., plane-stress) and beam element-based parameterization, although in the latter, the effect is not severe because of the presence of slender beam elements. Irrespective of the type of parameterization, there is a fundamental reason for the occurrence of lumped compliance. All the current force-deflection type formulations for topology optimization, in one form or another, simultaneously maximize the deformation at the output point and maximize the overall stiffness of the structure. These are called flexibility-stiffness formulations. The measure of stiffness used is essentially related to the elastic strain energy stored in the deformed structure. The lower the strain energy, the stiffer the structure. As posed, a rigid-body linkage with revolute joints is the true optimum because it can generate large output motion for a given force and has the minimum (zero) strain energy. Expectedly, optimization algorithms generate solutions that emulate rigid-body linkages. While this is useful from one perspective, it is not so useful to realize practically viable compliant designs since the lumped compliance limits the range of motion and leads to high, localized stresses. Thus, there is a need to understand why this happens and how to rectify it in order to get truly distributed compliant mechanisms. This is the topic of this article.

Organization of the Article

In Sec. 2, the reason for the appearance of lumped compliance in topologies generated using the current formulation is explained. In Sec. 3, two methods to avoid lumped compliance are presented. The first method, based on ‘‘filtered distortion energy’’ barely avoids lumped compliance and does not give the intended distributed compliance. The second method is based on a new kinematics objective function that guarantees distributed compliance. The outline of the sensitivity analysis and the solution method is presented in Sec. 4. Numerical examples are in Sec. 5, where results of earlier formulations and the new formulations are compared. The article ends with conclusions in Sec. 6.

POINT FLEXURES

Consider another example, shown in Fig. 3, where the compliant topology solution is a multilink mechanism with many flexural pivots. These pivots are point flexures where two plane-stress (or plane-strain) elements diagonally meet at a point. Even the seemingly distributed compliant segment consists of several point flexures. As noted earlier, the optimization algorithm prefers them because they make way for large displacements while not adding to the strain energy. A typical objective function used in these formulations is the ratio of output displacement to the strain energy (Frecker et al., 1997; Nishiwaki et al., 1998; Saxena and Ananthasuresh, 2000), which is maximized. Although point flexures help optimize the objective function as posed, they lead to some difficulties in practice.

The first difficulty is concerned with manufacturing. Living hinges found in plastic consumer products is one possibility but that is not the best solution because of high, localized stresses. In Pedersen et al. (2001), it was suggested that the hinges be replaced with short and narrow beams. This replacement increases the stiffness much more than what the point flexure originally had and decreases the output displacement in the modified design. The second difficulty is due to large stresses in only a

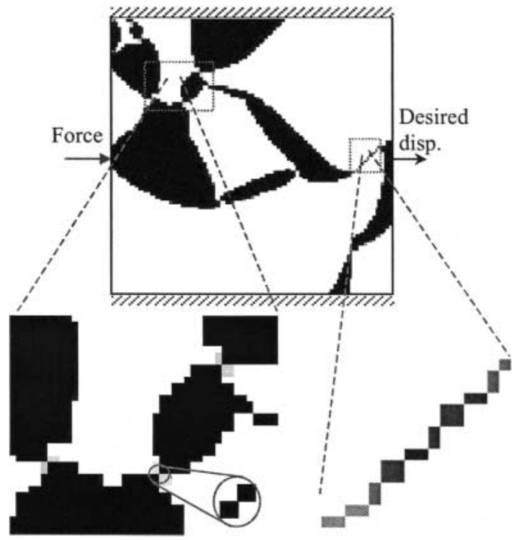

Figure 3. Point flexures in compliant topologies.

small portion of the mechanism. This is the antithesis of distributed compliance. So, point flexures must be avoided.

Including a stress constraint is not effective because in the finite element models used in the optimization procedure, the stresses at these sites are not usually large compared with, for example, the stresses where the mechanism is anchored to the fixed frame. A question might also arise as to whether a point flexure is really a pure kinematic hinge in the finite element model. That is, is there any stiffness associated with it? In order to study this, a square domain, shown in Fig. 4a, was discretized and analyzed in ABAQUS® (ABAQUS). The square is divided into four regions with Young's modulus E_0 in the top-left and bottom-right regions, and $E = \rho^{\eta} E_0$ in the top-right and bottom-left regions. This leads to a point flexure at the center of the square when ρ^{η} is sufficiently small. The right edge of the bottom-right region is fixed, and a force is applied at the top-left corner of the square.

With $\eta = 3$ and for different values of ρ, the square region was analyzed to simulate to see what happens in the finite element model of optimization. Figure 4b shows the ratio of the deflection at the top-left corner (U_2) of the square to half the length of the square (L_0) plotted against the ratio E/E_0. As can be seen, the flexibility of the point flexure rapidly increases as the ratio E/E_0 is decreased. In topology optimization, ρ^{η} is not permitted to go to zero because it leads to numerical

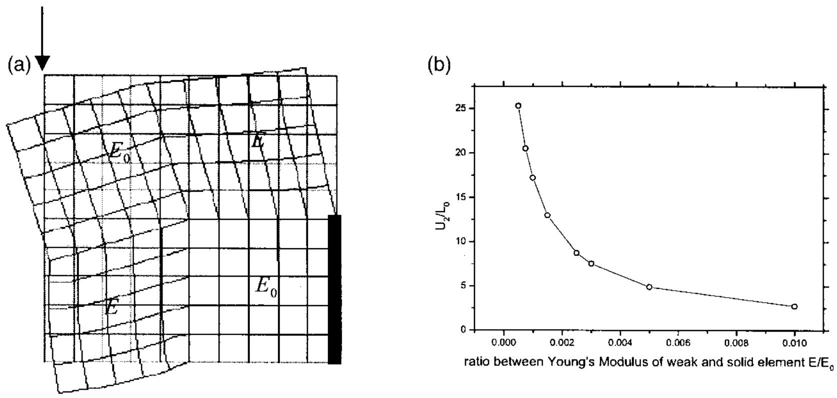

Figure 4. A test example to study point flexures (a) model of a test structure; (b) nondimensional deformation of the bottom-left point of the square to E/E_0.

problems in finite element solution. Usually, a small value such as 10^{-5} or 10^{-6} is chosen. The elements that reach these values "do not exist" in the design, which is really the essence of topology optimization. The plot in Fig. 4b indicates that even such "nonexiting" elements and all others with larger values of ρ^{η} do provide some stiffness at the point flexure, however small that may be. So, these are not pure kinematic hinges. A more interesting finding of this study was that point flexures do not necessarily experience large stresses. The conclusion then is that optimization algorithms are exploiting a loophole in the finite element model and the design parameterization of topology optimization to best optimize the objective function. It should be noted that when a beam element-based ground structure (Saxena and Ananthasuresh, 2000) is used instead of continuum elements, the same phenomenon exists but not as severely because fine discretizations usually are not used there.[a] The goal of this work is, therefore, to fix this loophole and avoid the point flexures.

TOWARD DISTRIBUTED COMPLIANCE

In order to guarantee distributed compliance in a new formulation, we must first have a quantitative definition for the distributed compliance

[a]In the beam element-based method, fine discretization will make the problem too big and is not necessary to define a topology or shape with enough detail.

that clearly distinguishes it from the lumped compliance. The intuitive notion of the distributed compliance is that "the stress (or the strain energy) is more or less uniformly distributed throughout the structure." Clearly, this is not the case in flexural pivot-based designs. Therefore, in order to avoid highly stressed regions, it is natural to impose an upper bound constraint on the state of stress (or strain energy) at every point that "exists"[b] in the design. However, this is not likely to work because of the occurrence of point flexures where stress (or strain energy) is not any larger than it is at other points. To emphasize this point, we first present a formulation that involves stress (or strain energy). As will be seen later, it helps in avoiding the point flexures only nominally. Therefore, even though the intuitive notion of more evenly distributed stress (strain energy) is correct, the finite element model does not capture that effectively because of point flexures. Consequently, a second formulation that penalizes point flexures successfully and helps eliminate them is proposed. The two formulations are presented next.

Filtered Distortion Energy Approach

The rationale behind this approach can be explained by comparing the currently used flexibility-stiffness formulations with the flexibility-strength formulation. In the latter, flexibility is maximized with an upper bound constraint on strength. The strength constraint can be imposed either as a local stress constraint [Eq. (1a)] at every point (Saxena and Ananthasuresh, 2001b) or in the integrated form [Eq. (1b)] (Duysinx and Bendsøe, 1998) as shown below.

$$\sigma(\mathbf{x}) - S^* \leq 0 \quad \forall\, \mathbf{x} \in \Omega \tag{1a}$$

$$\int_{\Omega} \sigma(\mathbf{x})^p \quad d\Omega \leq S^{*p} \tag{1b}$$

where

$\Omega =$ design region
$\sigma(\mathbf{x}) =$ stress matrix with all its components

[b]Recall that in topology optimization, all points are present all the time but only a few are thought to "exist" if the "material state" interpolated between 0 and 1 is more than 0 for them. A stress constraint imposed at every point must distinguish between existing and nonexisting points because unusually large stresses (stress singularities) are known to occur at nonexisting points (see Bruns and Tortorelli (2001) and the references therein).

$\mathbf{x}$ = any point in the design region
$\sigma(\mathbf{x})$ = any critical measure of the stress-state at a point such as the largest principal stress, the largest shear stress, or the von Mises stress
S^* = Yield strength

Local stress constraints lead to too many constraints (as many as the number of finite elements in the discretized model) and make the optimization problem computationally difficult to solve. Integrated constraints average out the stresses everywhere in the structure and hence cannot specifically penalize high stress regions. Therefore, we propose to filter out the critical regions, i.e., point flexures, and impose constraint only on those. Additionally, instead of using a stress, we use the distortion energy. Distortion energy is obtained by subtracting the hydrostatic strain energy from the total strain energy. The other way to understand this is by noting that the stress consists of two components, namely the hydrostatic component that effects change in volume, and the deviatoric component that effects distortion of the element. Indeed, the von Mises stress is derived on the basis of the distortion strain energy. So, the von Mises stress and the distortion energy are essentially equivalent when used in a constraint. The distortion strain energy de($\mathbf{x}$) at a point is given by

$$\mathrm{de}(\mathbf{x}) = \frac{1}{2}\mathbf{s}^{\mathrm{T}}\mathbf{C}\mathbf{s} \tag{2}$$

where
$\mathbf{s} = (\sigma - \mathbf{I}\,\mathrm{trace}(\sigma)/3)$ = deviatoric component of stress
$\mathbf{C}$ = strain-stress matrix

In the discretized finite element model, DE_i denotes the distortion energy of an element i. Since we only want to penalize the point flexures, a filter $\phi(\rho)$ shown below is used to automatically select such elements only.

$$\begin{aligned}\phi(\rho_i) = \frac{1}{4}\Bigg\{&\left(\frac{1}{1-(\rho_5-\rho_1)^2(\rho_5-\rho_4)^2(\rho_i-\rho_1)^2(\rho_i-\rho_4)^2}\right)^p \\ &+\left(\frac{1}{1-(\rho_6-\rho_1)^2(\rho_6-\rho_2)^2(\rho_i-\rho_1)^2(\rho_i-\rho_2)^2}\right)^p \\ &+\left(\frac{1}{1-(\rho_7-\rho_2)^2(\rho_7-\rho_3)^2(\rho_i-\rho_2)^2(\rho_i-\rho_3)^2}\right)^p \\ &+\left(\frac{1}{1-(\rho_8-\rho_3)^2(\rho_8-\rho_4)^2(\rho_i-\rho_3)^2(\rho_i-\rho_4)^2}\right)^p\Bigg\}\end{aligned} \tag{3}$$

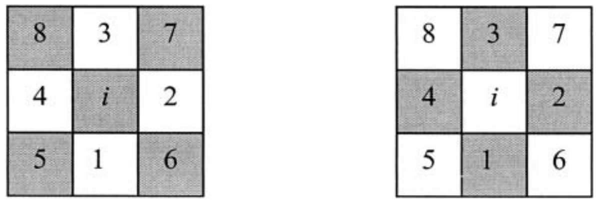

Figure 5. The numbering of neighboring elements used to define the filter function Eq. (3).

where p is a parameter chosen for a given problem (it is 4000 in the examples presented later). As can be seen in the above equation, whenever element i becomes a participant in a point flexure in any one of the eight configurations shown in Fig. 5, the filter function for that element becomes extremely large and is equal to one otherwise. The filtered distortion energy DE_f is then computed for the entire structure as follows.

$$\mathrm{DE}_f = \sum_{i=1}^{N} \phi(\rho_i)\mathrm{DE}_i \tag{4}$$

where N is the total number of finite elements.

The flexibility-strength formulation modified to penalize heavily point flexures can now be posed as follows. The objective function to be maximized is the mutual strain energy (MSE) (Saxena and Ananthasuresh, 2001), which is numerically equal to the output displacement under the applied load.

$$\begin{aligned}
&\text{Minimize} && -\mathrm{MSE} = -u_{\mathrm{out}} \\
&\text{w.r.t.} && \rho_i \ i = 1, 2, \ldots, N \text{ and } 0 < \rho_{\min} \leq \rho \leq 1 \\
&\text{Subject to} && \\
& && \sum_{i=1}^{N} \phi(\rho_i)\mathrm{DE}_i - \mathrm{DE}_f^* \leq 0 \qquad (5) \\
& && V = \sum_{i=1}^{N} \rho_i - V^* \leq 0
\end{aligned}$$

Alternatively, in efficiency-strength formulation (Saxena and Ananthasuresh, 2001), {sign(MSE)MSE^2/SE} is maximized instead of MSE under the same constraints. Here, SE is the strain energy, a measure of stiffness, and is equal to half of the sum of the displacements at which input forces are applied multiplied by the magnitudes of the corresponding forces. The design variable ρ_i is used to interpolate the state of the material using the simple isotropic material with penalty (SIMP) (Zhou and Rozvany, 1991) model by modifying the Young's modulus of the material E_0 as follows :

$$E_i = \rho_i^{\eta} E_0 \tag{6}$$

where η is a parameter to be chosen, typically as 3.

The sensitivity analysis and the solution algorithm that we used to solve the problem in Eq. (5) are not new because objective and constraints are continuous and are in the standard form. Therefore, only a brief outline of them is given in Sec. 4. Two examples are presented in the remainder of this section to show the efficacy of this formulation (or the lack of it). In both examples, a nonlinear finite element model that accounts for large deformation is used. Four-noded quadrilateral plane-stress elements are used for discretizing the design region.

Example 1, Using the Efficiency-Strength Formulation

The left two corners of a square design region of units 6×6 were fixed, and a force was applied at the center of the left edge toward right. The displacement was desired at the top-right and bottom-right corners downward and upward respectively. The design region was divided into 60×60 four-noded plane-stress elements with unit thickness. A volume constraint of 30% was used. The solution for the problem in Eq. (5) is shown in Fig. 6b. For the purpose of comparison, the same problem was solved without using the filter shown in Eq. (3), and its solution is shown in Fig. 6a. As can be seen in Fig. 6a, point flexure prevails when distortion energy at every existing point is included. The solution in Fig. 6b appears to be almost the same as Fig. 6a. But, if we closely observe the enlarged views of two portions, we see that the distortion energy filter has indeed worked but only nominally. That is, an extra element is present just to avoid a point flexure, but it is still a case of lumped compliance!

Example 2, Using the Flexibility-Strength Formulation

One more example was solved for different specifications but with the same data that was used in the previous example. The flexibility-strength formulation with the filtered distortion energy was used for this example. The solution is shown in Fig. 7. Once again, lumped compliance is not avoided, although point flexures were nominally absent.

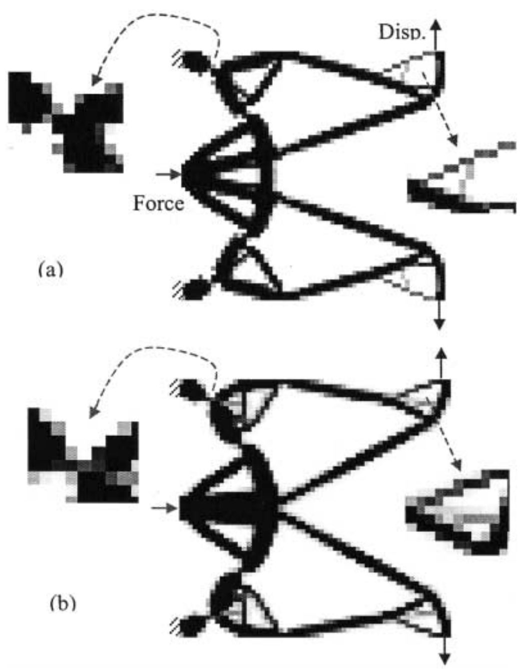

Figure 6. Example 1 (a) solution without using the filter for distortion energy; (b) solution with the filter. It can be seen that the filter avoided point flexures but did not give distributed compliance.

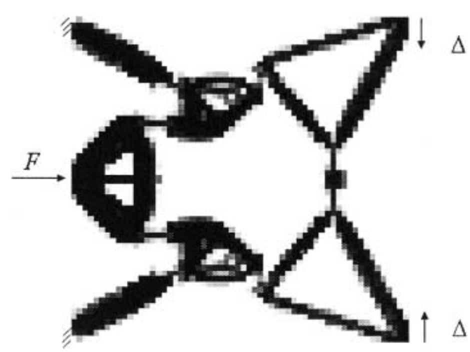

Figure 7. Solution for Example 2 with the filter for DE.

These, and several other examples we solved, clearly indicated that the distortion energy (or the stress constraint imposed in some other way), filtered to penalize the point-flexure elements or not, is not likely to give distributed compliance. With hindsight, it can be explained as follows. In compliant mechanisms, when analyzed using plane-stress elements, the hydrostatic part of the strain energy (SE) is only a small fraction of the total strain energy. So, making DE small is the same as making SE small. Since making SE small implies an increase in the stiffness, making DE small also implies an increase in the stiffness. But making DE, which is an integrated stress constraint, was supposed to increase the strength. There is no contradiction here if we recall that increasing the strength implies increasing the stiffness and vice versa for the same mode of deformation and under constant applied forces.[c] As noted earlier, formulations that intend to increase stiffness while maximizing flexibility tend toward lumped compliant designs. So, stress constraints alone do not lead to flexible and strong designs, and they fail to give distributed compliant designs. Next, we propose a novel formulation that guarantees distributed compliance.

Restrained Local, Relative Rotation Approach

The rationale for the approach presented in this section comes from an observation made earlier about the deformations caused by the point flexures. Since a point flexure emulates a revolute joint, there will be a substantially large relative rotation between the diagonally meeting elements at the point where they meet. This is evident in Fig. 4a and was seen in many other deformation patterns observed in our numerical experiments. Restraining the relative rotation by way of a penalty term in the objective function or constraint will, therefore, help prevent point flexures. If point flexures are prevented, emulating rigid-body linkages cease to be an option for optimization algorithms in flexibility-stiffness or flexibility-strength formulations. Consequently, it will pave the way for distributed compliance. Thus, we redefine the notion of distributed compliance based on the uniformity of the local, relative rotations at all

[c]This is not to say that stiffness and strength are the same. See Howell (2001; pp. 22–23) for an explanation of a situation when two different modes of deformation are considered. Consider also the case when loads change as the structure deforms, as in a wheat plant under wind loading. See Vogel (1995) for more examples of this kind. Furthermore, when the loads are displacements rather than forces, stiffness and strength are clearly distinguished.

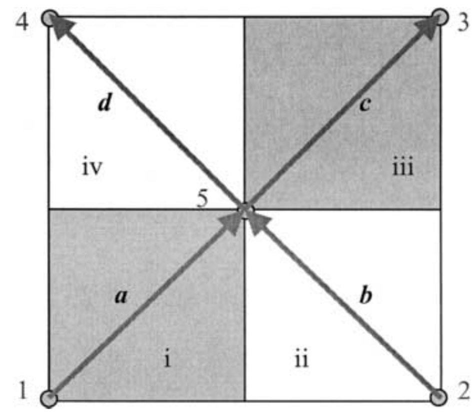

Figure 8. Notation used to quantify local, relative rotation.

existing points in the design region. The next task is to define this uniformity quantitatively in a manner that is amenable for the numerical implementation.

As shown in Fig. 8, consider four elements marked i, ii, iii, and iv with nodes marked 1 through 5, and four vectors, **a**, **b**, **c**, and **d**. It is easy to compute these four vectors for every node before and after the deformation. Now, the local relative rotation at every node can be quantified using cosines of two angles, α and β, and comparing their values before and after the deformation of the grid. That is, we consider:

$$\cos\alpha = \mathbf{a}\cdot\mathbf{c}/(\|\mathbf{a}\|\|\mathbf{c}\|) \text{ and } \cos\beta = \mathbf{b}\cdot\mathbf{d}/(\|\mathbf{b}\|\|\mathbf{d}\|) \tag{7a}$$

$$\{\cos\alpha_0 - \cos\alpha\} \text{ for shaded elements in Fig. 8}$$
$$\left\{\cos\beta_0 - \cos\beta\right\} \text{ for unshaded elements in Fig. 8} \tag{7b}$$

where the subscript zero refers to the angles computed with vectors **a**, **b**, **c**, and **d** in the undeformed configuration. Since the cosines of α and β are unity in the undeformed configuration for rectangular elements used in our examples, we get

$$\{1 - \cos\alpha\} \text{ for shaded elements in Fig. 8}$$
$$\{1 - \cos\beta\} \text{ for unshaded elements in Fig. 8} \tag{8}$$

If a node lies on a boundary and has a boundary condition imposed on it, only two of the vectors, **a** and **b** or **c** and **d**, can be defined, and, hence, the cosines of the angles are computed as:

$$\cos\alpha = \mathbf{a}\cdot\mathbf{a}_0/(\|\mathbf{a}\|\|\mathbf{a}_0\|) \text{ and } \cos\beta = \mathbf{b}\cdot\mathbf{b}_0/(\|\mathbf{b}\|\|\mathbf{b}_0\|)$$
or
$$\cos\alpha = \mathbf{c}\cdot\mathbf{c}_0/(\|\mathbf{c}\|\|\mathbf{c}_0\|) \text{ and } \cos\beta = \mathbf{d}\cdot\mathbf{d}_0/(\|\mathbf{d}\|\|\mathbf{d}_0\|) \tag{9}$$

Uniformity of α and β across all the nodes would ensure distributed compliance. In order to quantify this uniformity, the following (in) equality is used (see the appendix for a proof):

$$\sum_{i=1}^{N}(1-\cos\alpha_i) \geq N(1-\cos\overline{\alpha}) \tag{10}$$

where N is the number of the nodes, and $\overline{\alpha}$ is the arithmetic mean of all the α_i, and $-\pi/2 \leq \alpha_i \leq \pi/2$ holds good. The same inequality holds good for βs as well. This shows that when αs are different from each other, the sum of their cosines subtracted from unity is always larger than its value if they were to be all equal. When all of α are equal, the equality sign strictly holds good in Eq. (10). In order to have the compliance distributed, αs need to be as uniform as possible. Therefore, a combined measure that quantifies this ideal situation effectively should be minimized. Minimizing the standard deviation of the α is one way to achieve it. However, since the formerly used flexibility-stiffness formulation prefers to localize the deformation, it is also necessary that the change in the α be made small. Toward this end, if we minimize the left-hand-side term of Eq. (10), we drive the α_i to be as small as possible, and to be, by the argument presented above and the quantitative measure presented below, as uniform as possible too. With this background, we now define an objective function as follows.

$$\text{Minimize } \psi = -\frac{\text{MSE}}{\sqrt{\sum_{k=1}^{N}\left\{\varphi(\rho_{\mathrm{i}})\varphi(\rho_{\mathrm{iii}})(1-\cos\alpha_k)+\varphi(\rho_{\mathrm{ii}})\varphi(\rho_{\mathrm{iv}})(1-\cos\beta_k)\right\}}} \tag{11}$$

where the filter functions are defined as

$$\varphi(\rho) = 1-\exp\left(-\frac{\rho^2}{\mu^2}\right) \tag{12}$$

where the numerals i, ii, iii, and iv refer to the elements adjacent to the node k as shown in Fig. 8. The purpose of the filter is to exclude the elements that have reached their nonexisting state. The radical is included in Eq. (11) to make the denominator to be the same order of magnitude as the numerator. Other powers may also be used as deemed necessary. The parameter μ is chosen to make the filter extremely selective in penalizing only the "existing" elements. The optimization problem can now be stated as:

$$\begin{aligned} &\text{Minimize} && \psi \\ &\text{w.r.t.} && \rho_i \text{ where } i = 1, 2, \ldots, N \text{ and } 0 < \rho_{\min} \leq \rho \leq 1 \\ &\text{Subject to} && \sum_{i=1}^{N} (\mathrm{DE}_i) - \mathrm{DE}^* \leq 0 \\ & && \sum_{i=1}^{N} \rho_i - V^* \leq 0 \end{aligned} \tag{13}$$

The above problem statement accounts for the uniformity of local, relative rotations that would ensure the distributed compliance (denominator of ψ), maximizing the flexibility (numerator of ψ), containing the stress levels (the constraint on DE), and obeying the volume constraint (constraint on V).

AN OUTLINE OF THE SOLUTION METHOD

It should be noted that the proposed objective function and constraints maintain the continuity (up to and exceeding C^1) in terms of the design variable ρ. Therefore, the analytical sensitivity analysis can be accomplished easily using the standard procedures (Haftka and Gurdal, 1989) albeit with much algebraic manipulation (Yin and Ananthasuresh, 2001; Yin and Yang, 2001). Given the nonlinearity of the constraints, the sequential linear programming (SLP) was used to solve the problems stated in Eqs. (5) and (13). Details are not given here because they can be found in the literature including many books (e.g., Saxena et al. (2000)).

The optimality criteria method could have been used with the appropriate inner loop to update the Lagrange multipliers corresponding to the nonlinear constraints. The linearization done in SLP circumvents this problem. The other types of mathematical programming methods such as sequential quadratic programming, method of moving asymptotes, etc., may also be used.

NUMERICAL EXAMPLES AND DISCUSSION

The examples presented in this section were solved using the linear deformation theory for simplicity. Each of the three example problems (3, 4, and 5) was solved first using the flexibility-strength (with filtered distortion energy) formulation and then with the new formulation of Eq. (13). The results are shown in Figs. 9–11. The force and the directions of the desired output displacement are shown in each figure, which constitutes the problem specification. The remaining data for these examples is the same as that of Example 1 presented earlier. The specific values of force used and the displacements obtained are irrelevant in topology optimization, especially when linear deformation theory is used. It is the deformation pattern that is important. So, each example shows the deformation pattern. It can be seen that in all cases, the point flexures disappeared, giving rise to the distributed-compliant segments in the topologies resulting from the new formulation. It is also evident from the deformation patterns (Figs. 9d and 10d) that deformation is more uniformly distributed than it is in their lumped-compliant solutions (Figs. 9a and 10a). Although it may seem that distributed-compliant solutions (Figs. 9b, 10b, and 11b) had smaller output displacements than those of the lumped-compliant solutions (Figs. 9a, 10a, and 11a), when smoothened solid models or the physical prototypes are created, the lumped-compliant designs are bound to have smaller output displacements. Quantitative evaluation of these designs is presented next. It should also be noticed that for some problem specifications, truly distributed compliance might not be achievable. Example 5, shown in Fig. 11, is one such case. This can be attributed to either the nature of this problem specification and the data or the inability of the optimization algorithm in finding a better local minimum. This is not a limitation of the problem formulation because the distributed compliance is intrinsically present in it.

Quantitative Comparison of Lumped- and Distributed-Compliant Topologies

In order to see the effectiveness of the part of the objective function related to the averaged local, relative rotation used in Eq. (11), we plot the frequency of occurrence of a value of $(1 - \cos(\alpha))$ in the designs of

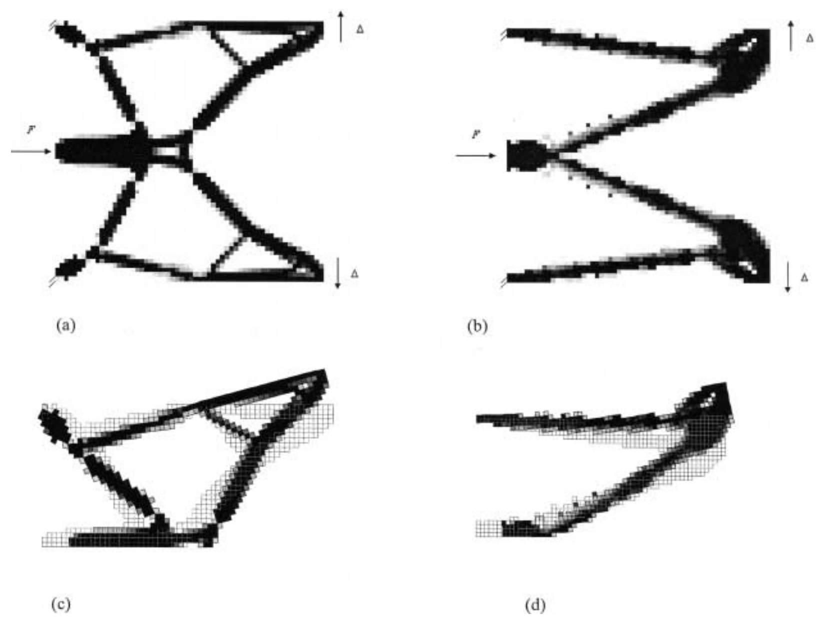

Figure 9. Example 3 (a) solution obtained using old flexibility-stiffness formulation; (b) distributed compliant topology obtained using new formulation [Eq. (13)]; (c) deformation of solution in (a); (d) deformation of solution in (b).

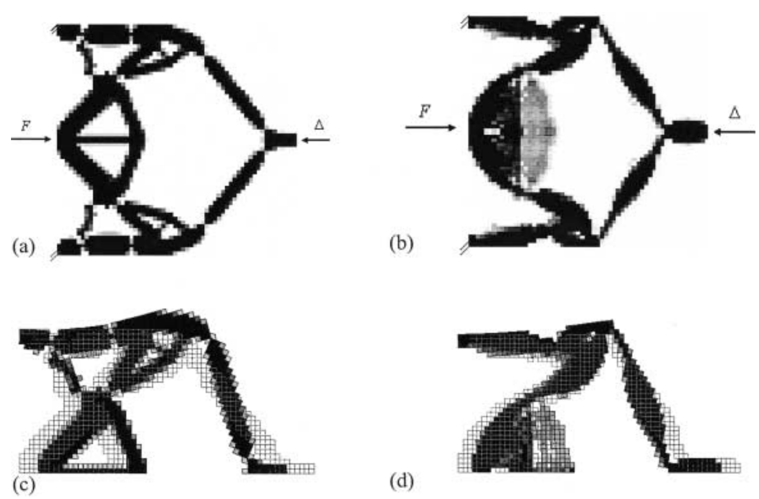

Figure 10. Example 4 (a) solution obtained using old flexibility-stiffness formulation; (b) distributed compliant topology obtained using new formulation [Eq. (13)]; (c) deformation of solution in (a); (d) deformation of solution in (b).

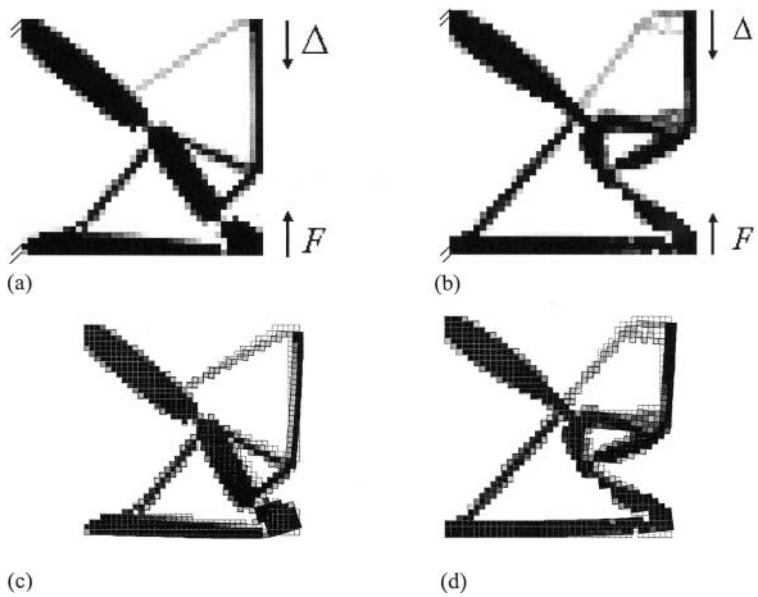

Figure 11. Example 5 (a) solution obtained with old flexibility-stiffness formulation; (b) distributed compliant topology solution with the new formulation of Eq. (13); (c) deformation of solution in (a); (d) deformation of solution in (b).

Figs. 9a and 9b shown in Fig. 12. The log scale used in the figure necessitated unity to be added to frequency because there are several values of $(1-\cos(\alpha))$ whose frequency was zero. As can be seen from Fig. 9a, the nonuniformity of $(1-\cos(\alpha))$ across all nodes in this design is shown in Fig. 12a, where large values of $(1-\cos(\alpha))$ are limited to a few nodes, while the other nodes have very small values, lying in the range (0, 0.0025). These later nodes belong to the portions that behave like rigid parts. This shows that Fig. 12a is a lumped-compliant mechanism with several flexural pivots. On the other hand, the frequency graph of the distributed compliant mechanism of Fig. 9b is much more uniform, with values of $(1-\cos(\alpha))$ lying in the range (0, 0.0025) for all nodes. This quantitatively validates the use of the objective function shown in Eq. (11).

Earlier in the paper, two problems were cited with lumped-compliant topologies, even if there is a way to manufacture them by replacing point flexures with short and narrow beams. First, since point flexures in the finite element model have very little stiffness, when we replace them with short and narrow beams, the mechanism becomes much stiffer, moving even farther from the compliant and strong paradigm of compliant mechanisms. Second, the stresses are localized to small regions, and the

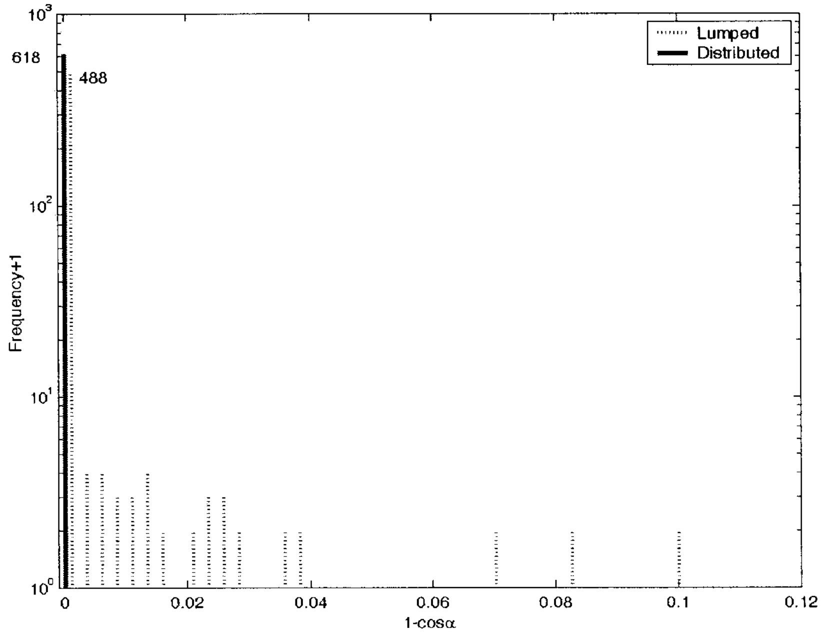

Figure 12. Frequency of occurrence of $(1 - \cos(\alpha))$ in lumped and compliant designs.

maximum stress in them is larger than it is in their distributed-compliant counterparts. In order to verify this, the solutions of the three examples were modeled in a solid modeling software program I-DEAS (I-DEAS, 2000) and analyzed using ABAQUS. The set of data for these examples was as follows: thickness = 3 mm; size 150×150 mm for the first two examples and 75×75 mm for the third; the Young's modulus is 2 GPa and the Poisson's ratio is 0.33. Figures 13a, 14a, and 15a show the deformation patterns, which make it clear that the results of the new formulation indeed possess the distributed compliance. Figures 13b, 14b, and 15b show the deformation at the output for the lumped- and distributed-compliant mechanisms for the same force. Distributed-compliant mechanisms are generally more flexible than the lumped-compliant counterparts as can be seen in the figures. Furthermore, Figures 13c, 14c, and 15c show the maximum stress, from which it is clear that the stress levels are smaller in distributed-compliant designs. Although Fig. 13b shows that distributed-compliant mechanism has larger stress than that of the lumped-compliant mechanism, it should be noted that the deflection in the distributed design is about 10 times more than that in

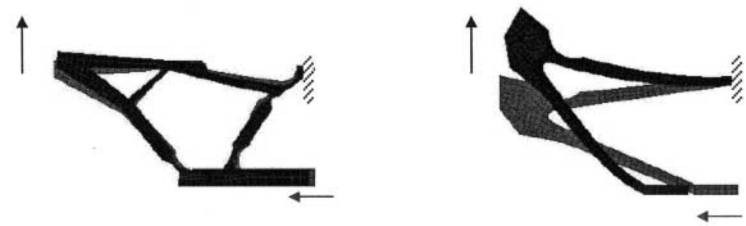

(a) (b)

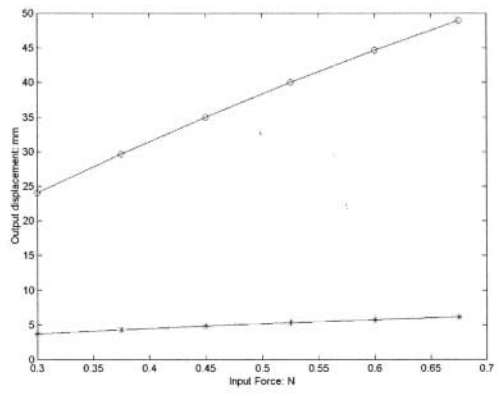

(c)

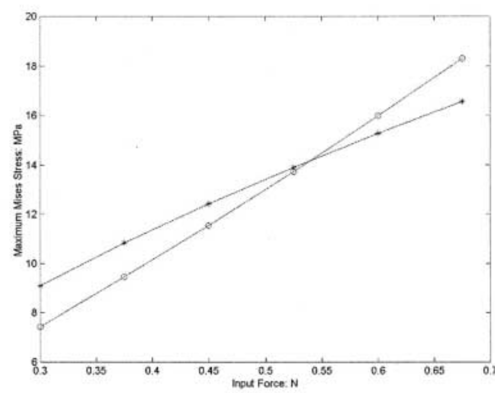

(d)

Figure 13. Quantitative analysis of distributed-compliant solutions of Example 3. (a) solid model of lumped-compliant design of Fig. 9a; (b) solid model of distributed-compliant design of Fig. 9b; (c) output displacement vs. force; (d) maximum stress vs. force.

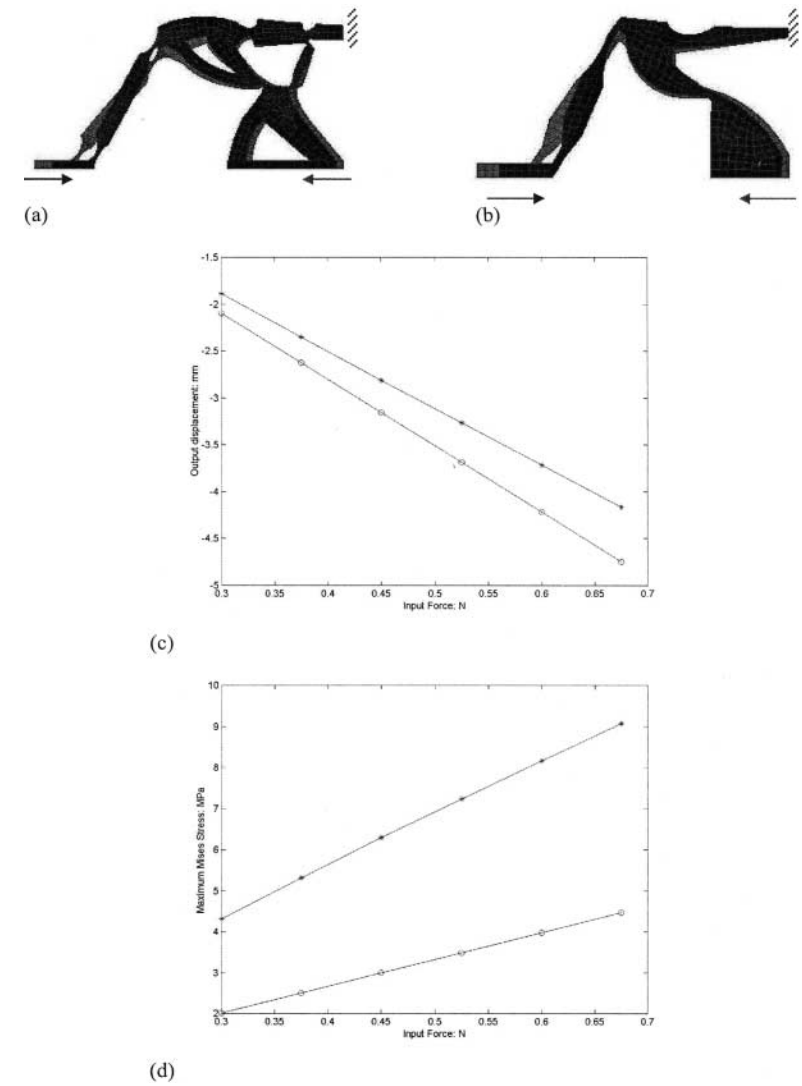

Figure 14. Quantitative analysis of distributed-compliant solutions of Example 4. (a) solid model of lumped-compliant design of Fig. 10a; (b) solid model of distributed-compliant design of Fig. 10b; (c) output displacement vs. force; (d) maximum stress vs. force.

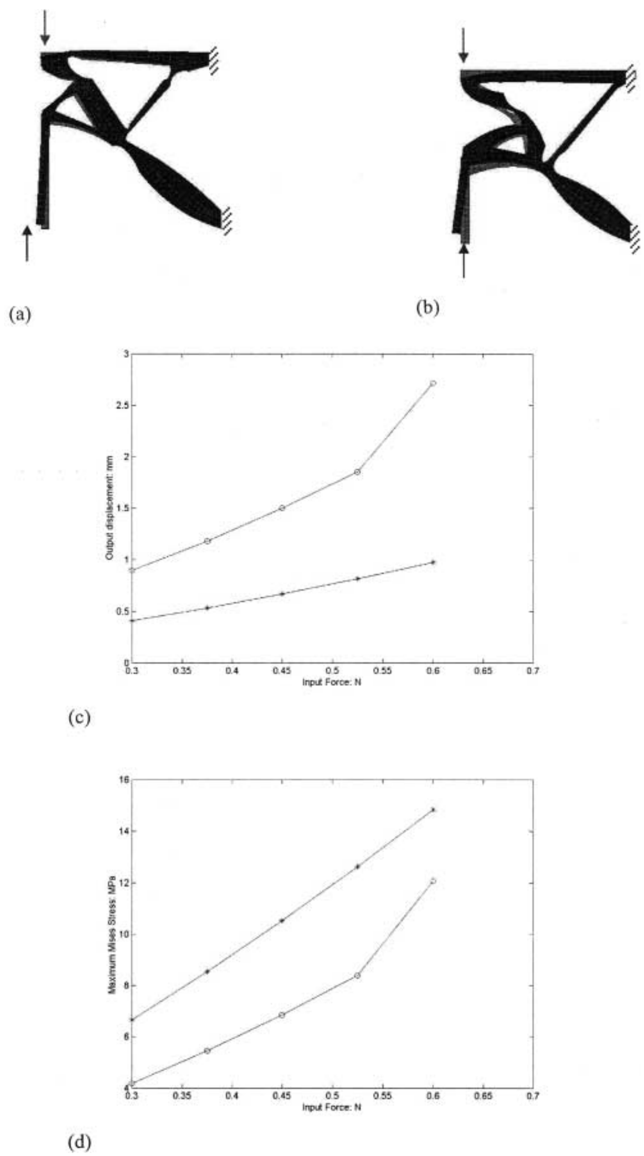

Figure 15. Quantitative analysis of distributed-compliant solutions of Example 3. (a) solid model of lumped-compliant design of Fig. 11a; (b) solid model of distributed-compliant design of Fig. 11b; (c) output displacement vs. force; (d) maximum stress vs. force.

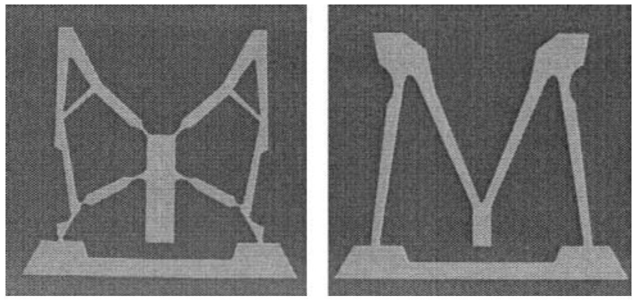

Figure 16. Polypropylene hand-actuated prototypes of lumped- and distributed-compliant mechanisms of Example 3 (Figs. 9a and 9b; and 12a and 12b).

the lumped design for the same force. Therefore, if we plot the maximum stress against output displacement, the distributed solution would look better, even in this case.

Prototypes

It can be seen that topology images obtained from the optimization procedure were closely adhered to in creating the solid models, except, of course, replacing point flexures with narrow and short beams, keeping our prototyping ability in mind. The lumped- and distributed-compliant solutions of Example 3 were prototyped at the macro scale using 0.125 in thick polypropylene sheets and machining them on a CNC milling machine. Both are of the same size and roughly of the same volume of material. The photographs of the prototypes are shown in Fig. 16. The quantitative analysis presented above was confirmed when these two prototypes were manually actuated. In particular, the distributed-compliant mechanism is more flexible than the lumped-compliant mechanism. This can be felt by noticing how much force is to be applied to cause a certain displacement at the output.

CLOSURE

Current topology optimization formulations for compliant mechanisms lead to lumped-compliant designs where flexibility is limited to a few flexural pivots, while the rest of the structure is rigid. This was due to the way the problem was posed and the type of design parameterization used in the numerical optimization procedure. Lumped-compliant designs suffer from high, localized stresses. If the flexural pivots are made stronger by modifying their geometry, the mechanism would suffer from the increased stiffness. In this article, two methods were suggested to overcome this, after identifying the source of the problem. The first method, which penalized high-stressed regions using filtered distortion energy, is not successful in giving distributed-compliant designs. This shows that the way topology optimization is numerically implemented is not appropriate to properly define distributed compliance in terms of distributed stress or strain energy. The second method uses local, relative rotation and restrains it using a novel objective function that hopes to make the local deformation uniform throughout the structure. This shows the potential to give truly distributed-compliant designs. Numerical examples and some quantitative analysis of the obtained designs that demonstrate the usefulness of the new formulation are also presented.

APPENDIX

Proof of the (in)equality in Eq. 10.

Taylor series expansion of $\cos(\alpha_i)$ about $\overline{\alpha}$ up to one term with the remainder in Lagrange's form is given by

$$\cos(\alpha_i) = \cos(\overline{\alpha}) - \sin(\overline{\alpha})(\alpha_i - \overline{\alpha}) - \frac{1}{2}\cos(\xi_i)(\alpha_i - \overline{\alpha})^2 \tag{A1}$$

where $\overline{\alpha}$ is the arithmetic mean of α_i, $i = 1, 2, \ldots, N$ and ξ_i is a value between $\overline{\alpha}$ and α_i. Then,

$$\sum_{i=1}^{N}\cos(\alpha_i) = N\cos(\overline{\alpha}) - \sin(\overline{\alpha})\sum_{i=1}^{N}(\alpha_i - \overline{\alpha}) - \frac{1}{2}\sum_{i=1}^{N}\cos(\xi_i)(\alpha_i - \overline{\alpha})^2 \tag{A2}$$

The second term on the right-hand side in the above equation is zero by definition of the arithmetic mean. Since, $\cos(\xi_i)$ is positive for the range $-\pi/2 \le \xi_i \le \pi/2$, we can write the following from Eq. (A2):

$$\sum_{i=1}^{N}\cos(\alpha_i) \le N\cos(\overline{\alpha}) \tag{A3}$$

from which we get

$$\sum_{i=1}^{N} (1 - \cos(\alpha_i)) \geq N(1 - \cos(\overline{\alpha})) \tag{A4}$$

which proves the (in)equality of Eq. (10).

ACKNOWLEDGMENTS

The authors are grateful to the National Science Foundation for providing the financial support for this work with a grant (DMI-9800417). Many valuable discussions with Mr. Nilesh Mankame, and the insightful comments made by the anonymous reviewers, which improved the writing of this article, are also gratefully acknowledged.

REFERENCES

ABAQUS. Finite Element Software from HKS, Inc., www.abaqus.com.

Ananthasuresh, G. K., Kota, S. (1995). Designing Compliant Mechanisms. *Mechanical Engineering* 117(11):93–96.

Bruns, T. E., Tortorelli, D. A. (2001). Topology optimization of non-linear elastic structures and compliant mechanisms. *Computer methods in Applied Mechanics and Engineering* 190 (26–27):3443–3459.

Burns, R. H., Crossley, F. R. E. (1968). Kinetostatic Synthesis of Flexible Link Mechanisms. ASME Paper No. 68-MECH-36.

Duysinx, P., Bendsøe, O. (1998). Topology optimization of continuum structures with local stress constraints. *International Journal for Numerical Methods in Engineering* 43(2):1453–1478.

Forster, M. P. (2000). Constructieprincipes (in Dutch), University of Twente Press: The Netherlands.

Frecker, M., Ananthasuresh, G. K., Nishiwaki, S., Kikuchi, N., Kota, S. (1997). Topological synthesis of compliant mechanisms using multi-criteria optimization. *ASME Journal of Mechanical Design* 119(2):238–245.

Haftka, R. T., Gurdal, Z. (1989). *Elements of Structural Optimization*. Boston: Kluwer Academic Pubishers.

Her, I., Midha, A. (1987). A compliance number concept for compliant mechanisms, and type synthesis. *Journal of mechanisms, Transmissions, and Automation in Design* 109(3):348–355.

Howell, L. L. (2001). *Compliant Mechanisms*. New York: John Wiley and Sons, Inc.

Howell, L. L., Midha, A. (1994). A method for the design of compliant mechanisms with small-length flexural pivots. *ASME Journal of Mechanical Design* 116(1):280–290.

Howell, L., Midha, A. (1996). A loop-closure theory for the analysis and synthesis of compliant mechanisms. *ASME Journal of Mechanical Design* 118(1): 121–125.

I-DEAS. (1997). I-DEAS, Master Series Ver. #3, Student Guide, Structural Dynamics Research Corporation, 2000, Eastman Drive, Milford, OH 45150.

Lobontiu, N., Paine, J. S. N., Goldfarb, M., Garcia, E. (2001). Corner-filleted flexure hinges. *ASME Journal of Mechanical Design* 123(3):346–352.

Mettlach, G. A., Midha, A. (1996). Using Burmester theory in the design of compliant mechanisms. In: Proceedings of the 1996 ASME Design Engineering Technical Conferences, 96-DETC/MECH-1181.

Nishiwaki, S., Frecker, M. I., Min, S., Kikuchi, N. (1998). Topology optimization of compliant mechanisms using the homogenization method. *International Journal of Numerical Methods in Engineering* 42:535–559.

Paros, J. M., Weisbord, L. (1975). How to design flexure hinges. *Machine Design* Nov. 25, 1965, 151–156.

Pedersen, C. B. W., Buhl, T., Sigmund, O. (2001). Topology synthesis of large-displacement compliant mechanisms. *International Journal for Numerical Methods in Engineering* 50:2683–2705.

Saxena, A., Ananthasuresh, G. K. (2000). On an optimal property of compliant mechanisms. *Structural and Multidisciplinary Optimization* 19:36–49.

Saxena, A., Ananthasuresh, G. K. (2001a). Topology synthesis of compliant mechanisms for nonlinear force-deflection and curved path specifications. *Journal of Mechanical Design* 123:33–42.

Saxena, A., Ananthasuresh, G. K. (2001b). Topology design of compliant mechanisms with strength considerations. *Mechanics of Structures and Mechanisms* 29(2):199–221.

Saxena, A., Ananthasuresh, G. K. (2003). A computational approach to number synthesis of linkages. *Journal of Mechanical Design* 125:110–118.

Saxena, A., Wang, X., Ananthasuresh, G. K. "PennSyn—A Topology Synthesis Software for Compliant Mechanisms," DETC/MECH-14139, ASME Design Engineering and Technical Conference, Sept. 2000, Baltimore, MD.; http://www.seas.upenn.edu/~gksuresh/.

Shoup, T. E., McLarnan, C. W. (1971). On the use of undulating elastica for the analysis of flexible link mechanisms. *Journal of the Engineering for Industry*, *Transactions of the ASME* 1971, Feb., pp. 263-267.

Sigmund, O. (1997). On the design of compliant mechanisms using topology optimization. *Mechanics of Structures and Machines* 25(4):495–526.

Sigmund, O. (2001). Designing of multiphysics actuators using topology optimization-Part I: one-material structures. *Computer Methods in Applied Mechanics and Engineering* 190:6577–6604.

Silva, E. C. N., Nishiwaki, S., Kikuchi, N. (2000). Topology optimization design of flextensional actuators. *IEEE Transactions on Ultrasonics*, *Ferroelectrics*, *and Frequency Control* 47(3):657–671.

Smith, S. T., Chetwynd, D. G. (1994). *Foundations of Ultra-Precision Mechanism Design*. Francis and Taylor.

TOPOPT, http://www.topopt.dtu.dk/.

Tuttle, S. B. (1967). *Mechanisms for Engineering Design*. New York: John Wiley and Sons, Inc.

Vogel, S. Better bent than broken. Discover, May, 1995, 62–67.

Waldron, K. J., Kinzel, G. (2000). *Kinematics*, *Dynamics*, *and Design of Machinery*. New York: John Wiley and Sons, Inc.

Yin, L., Ananthasuresh, G. K. (2001). Topology optimization of compliant mechanisms with multiple materials using a peak function material interpolation scheme. *Structural and Multidisciplinary Optimization* 23(1):49–62.

Yin, L., Ananthasuresh, G. K. (2002). Novel design technique for electro-thermally actuated compliant micromechanisms. *Sensors and Actuators*, *A Physical* 97–98, 599–609.

Yin, L., Yang, W. (2001). Optimality criteria method for the topology optimization under multiple constraints. *Computers and Structures* 79:1839–1850.

Zhou, M., Rozvany, G. I. N. (1991). The COC Algorithm. Part II: topological, geometrical, and generalized shape optimization. *Comp*. *Meth*. *Appl*. *Mech*. *Engrg*. 89:309–336.

Received July 2002
Revised January 2003
Communicated by S. Azarm